Int. J. Solids Structures, 1970, Vol. 6, pp. 553 to 568. Pergamon Press. Printed in Great Britain

A THEORETICAL AND EXPERIMENTAL INVESTIGATION OF IMPULSIVELY LOADED CLAMPED CIRCULAR VISCOPLASTIC PLATES

T. WIERZBICKI

Institute of Basic Technical Research, Warsaw, Poland

and

A. L. FLORENCE

Stanford Research Institute, Menlo Park, California

Abstract—Experiments are described in which clamped circular plates of 6061-T6 aluminum alloy and H.R. steel A285 were subjected to uniformly distributed impulses to cause permanent central deflections ranging from one to several plate thicknesses. A viscoplastic theory of plates is presented that takes into account large deflections; the theory includes the rigid–perfectly plastic plate as a special case. By correlating predicted and experimental permanent deflections of the strain-rate insensitive aluminum and the strain-rate sensitive steel plates it is found that the effects of large deflections (which give rise to significant membrane forces) and strain-rate sensitivity are comparably responsible for the deflections being below those predicted by the bending theory of rigid–perfectly plastic plates.

INTRODUCTION

A SIMPLE formula for the permanent central deflection of a simply supported circular plate caused by a uniformly distributed impulse was obtained by Wang [1] from rigid–perfectly plastic bending theory. By comparing these predicted deflections with experimental results Florence [2] found that the greater the deflection the greater was the overestimation. Because the plate materials (6061-T6 aluminum and C.R. steel 1018) are insensitive to strain-rate the strengthening with deflection was attributed to the buildup of membrane forces. Jones [3] analysed the simply supported circular plate taking membrane forces into account and found good agreement with experimental deflections. Wierzbicki [4] showed that deflection predictions of the rigid–perfectly plastic bending theory can be improved by taking strain-rate sensitivity into account and demonstrated this by correlation of the deflections predicted from a viscoplastic theory and the deflections of C.R. steel 1018 plates [2], (this material has some strain-rate sensitivity). Other investigations of the strengthening effects of strain-rate sensitivity include those of Perrone [5], Jones [6], Kelley and Wilshaw [7], and Wierzbicki [8].

The present investigation aims at determining the contributions of strain-rate sensitivity and geometry changes to the strengthening of clamped circular plates, relative to the rigid–perfectly plastic bending theory of Wang and Hopkins [9]. Again, the plates are subjected to uniformly distributed impulses. The two materials chosen for the experiments are 6061-T6 aluminum alloy and H.R. steel A285, the former because it is insensitive to

strain rate and the latter because it is sensitive to strain rate. This choice allows a separation of strain-rate and geometrical effects. Another reason for the choice of materials is that the strain-hardening moduli are small enough to disregard.

The postulated viscoplastic theory contains the following simplifying assumptions that permit the derivation of an explicit expression for the final deflected shape of a plate:

(i) the material behavior is linearly viscoplastic
(ii) the constitutive equations based on the Huber–Mises yield condition are approximated to yield linear relations between components of the generalized stress and strain-rate vectors
(iii) only transverse displacements are taken into account

The reasonably good agreement between predicted and experimental deflections over the entire loading range suggests that the postulated theory describes the plate response. It is concluded from the investigation that strain-rate sensitivity and membrane force buildup through large deflections contribute comparably to the strengthening of the steel plates.

DESCRIPTION OF EXPERIMENTS

Explosive loading experiments were performed with 13 plates of 6061-T6 aluminum alloy and 18 plates of H.R. steel A285, all nominally $\frac{1}{4}$ in. thick and $9\frac{3}{4}$ in. dia. Each plate was clamped to prevent rotation but not radial displacements by means of two heavy steel annuli with inner diameters of 8 in. Figure 1 shows the experimental arrangement. Around the rim of each plate at $\frac{3}{4}$ in. spacing, $\frac{5}{8}$ in. long slots were cut, so that circumferential membrane forces in the annular portion of plate outside the 8 in. dia. circle were suppressed. The slots are seen in Fig. 2, which is a photograph of two deformed aluminum plates (one of the plates has been sectioned along a diameter).

The above method of clamping was originally designed for an experiment to produce deflections for comparison with those predicted by a bending theory taking into account strain-rate sensitivity (this theory is described later as a special case). After the experiments were carried out the theory was extended to include large deflections. Experiments should be run with fully clamped plates. Nevertheless, comparisons are probably still meaningful because the membrane forces achieve their full value over a large central area of plate.

The uniformly distributed impulse was generated by sheet explosive† rolled to a uniform thickness and cut out to form a disk of 8 in. dia. This disk of explosive was placed centrally over a similar disk of solid neoprene attenuator which in turn was layed centrally over the plate. The neoprene served to reduce the shock wave pressure entering the plate, eliminate spalling, and to avoid possible changes of material properties. For the aluminum plates $\frac{1}{8}$ in. thick neoprene was found to be satisfactory. For the steel plates, in order not to affect the strain-rate sensitivity, $\frac{1}{2}$ in. thick neoprene was used; this thickness was sufficient to reduce the peak pressure of the wave from the explosive so that only an elastic wave entered the steel. Five grain mild detonating fuse was used to detonate the explosive. The detonation velocity (0·29 in/μsec) is supersonic relative to the plate velocity (0·21 in/μsec) and the initiation point is at the plate center, so it is assumed, by analogy with beam

† Detasheet D, manufactured by DuPont.

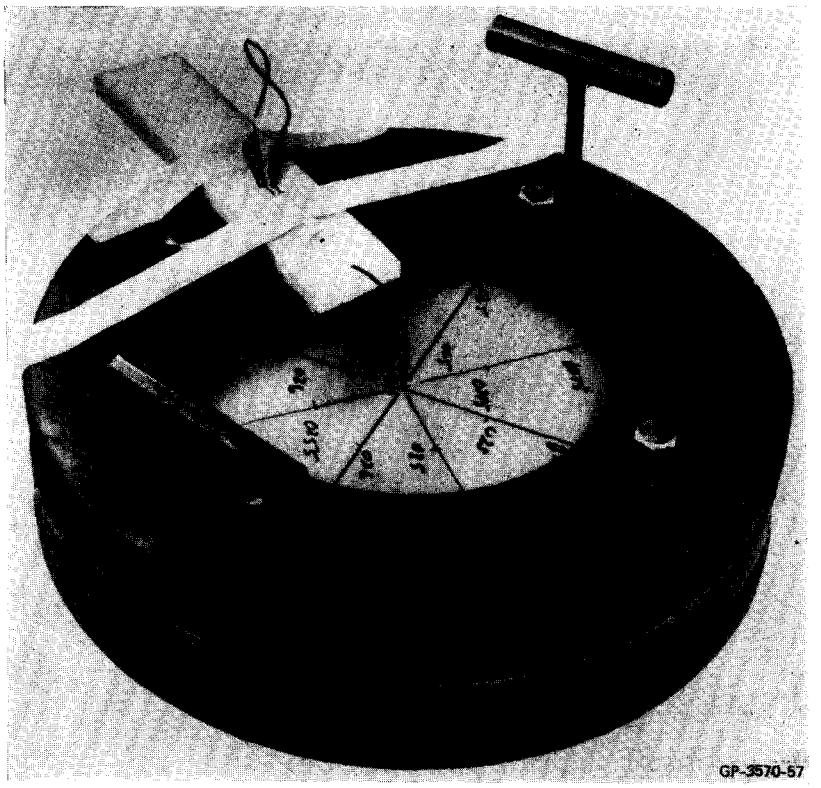

FIG. 1. Experimental arrangement.

facing p. 554

FIG. 2. Deformed plates of 6061—T6 aluminum alloy.

results [10], that an ideal impulse simultaneously applied over the whole plate is satisfactorily simulated by the rapidly expanding narrow ring of high pressure at the detonation front.

For the explosive-attenuator-plate configurations, the impulse imparted was obtained by projecting free 8 in. dia. plates in front of a double-flash X-ray unit. The rigid-body displacement in the predetermined time between radiographs gives the plate velocity and hence its momentum. It was found that the velocity imparted to the aluminum plates was proportional to explosive thickness over a range from 15 to 60 mils and resulted in a calibrated impulse of $I_0 = 635$ dyn sec/cm^2 per mil of explosive. These impulse calibration experiments were carried out in a previously reported study [2] of simply-supported plates. From 10 similar experiments with free 8 in. dia. steel plates and explosive thicknesses ranging from 20 to 60 mils it was found that the velocity imparted was not proportional to explosive thickness. A least square fit of the calibration points resulted in an impulse of $I_0 = 768 - 1{\cdot}14h_e$ dyn sec/cm^2 per mil of explosive, where h_e is the explosive thickness measured in mils.

To determine yield stress an average value was taken of static tensile tests with specimens cut with and across the grain. Each curve was fitted by two straight lines and the point of intersection determined the yield stress (this stress is higher than the yield stress obtained from commonly accepted definitions).

Permanent deflections of points along a diameter and changes of thickness in central and support regions were measured.

Table 1 contains the principal experimental data.

TABLE 1. EXPERIMENTAL DATA

Plate material	Yield stress (lb/in^2)	Density (g/cm^3)	Plate thickness (in.)	Plate radius (in.)	Attenuator material	Attenuator thickness (in.)	Impulse calibration (dyn sec/cm^2/mil)
Al 6061-T6	42,000	2·7	0·251	4	Solid neoprene	$\frac{1}{8}$	635
H.R. steel A285	41,080	7·8	0·245	4	Solid neoprene	$\frac{1}{2}$	$768-1{\cdot}14h_e$†

† h_e is the explosive thickness in mils.

EXPERIMENTAL RESULTS

The experimental central deflections δ_{ex} and the corresponding impulses I are listed in Table 2. Central deflections δ_{th} predicted by the rigid–plastic bending theory [9] are given by

$$\delta_{th}/R = 0{\cdot}56\, I^2 R/8\mu M_0 \tag{1}$$

where R is the plate radius, μ the area density, and $M_0 = \sigma_0 h^2$ is the fully plastic moment, σ_0 being the yield stress and $2h$ the plate thickness. The experimental and theoretical central deflections are shown in Fig. 3, with convenient dimensionless scales based on the above solution.

Both sets of experimental deflections are below the straight line of the bending theory and have trends indicating plate strengthening with increasing impulse. Because the aluminum alloy is insensitive to strain rate, strengthening is due to buildup of membrane

TABLE 2. EXPERIMENTAL RESULTS

Material	Experiment no.	Impulse I (lb sec/in^2)	Impulse I (dyn sec/cm^2)	Central deflection radius $\delta ex/R$	$\delta ex/(\delta th)_{WH}$†
Al 6061-T6	1	0·268	18,500	0·264	0·538
	2	0·238	16,400	0·230	0·591
	3	0·238	16,400	0·229	0·589
	4	0·228	15,700	0·221	0·619
	5	0·228	15,700	0·216	0·610
	6	0·212	14,600	0·207	0·674
	7	0·202	14,000	0·185	0·658
	8	0·196	13,500	0·181	0·688
	9	0·180	12,400	0·154	0·700
	10	0·170	11,700	0·144	0·727
	11	0·162	11,200	0·134	0·744
	12	0·144	10,000	0·112	0·783
	13	0·144	9900	0·108	0·766
H.R. steel A285	1	0·615	42,400	0·280	0·290
	2	0·598	41,200	0·252	0·277
	3	0·559	38,600	0·249	0·312
	4	0·559	38,600	0·247	0·310
	5	0·507	35,000	0·220	0·335
	6	0·491	33,900	0·215	0·349
	7	0·471	32,500	0·210	0·371
	8	0·471	32,500	0·208	0·367
	9	0·424	29,200	0·183	0·398
	10	0·417	28,800	0·176	0·397
	11	0·379	26,100	0·152	0·415
	12	0·378	26,100	0·155	0·425
	13	0·332	22,900	0·128	0·453
	14	0·325	22,400	0·129	0·477
	15	0·270	18,600	0·080	0·429
	16	0·263	18,100	0·078	0·438
	17	0·206	14,200	0·050	0·463
	18	0·196	13,300	0·037	0·394

† $(\delta th)_{WH}$ is theoretical central deflection given by (1).

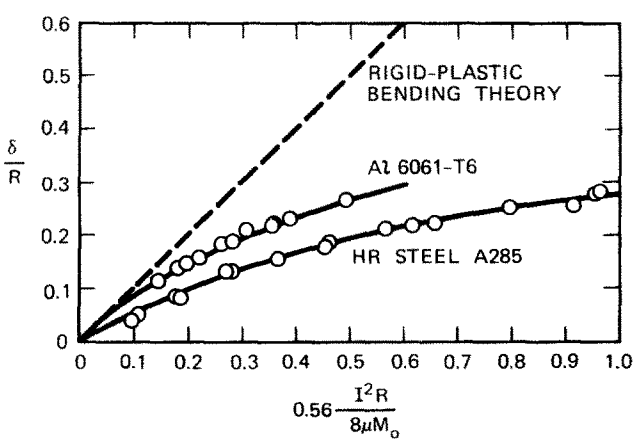

FIG. 3. Experimental and theoretical central deflections for clamped plates.

forces. The deflections for the steel plates lie below those for the aluminum plates indicating additional strengthening due to strain-rate sensitivity. Whenever deflections are such that $\delta/R < 0{\cdot}15$, strain-rate effects are larger than membrane effects, and whenever $\delta/R > 0{\cdot}15$, membrane effects are larger than strain-rate effects.

Figure 4 shows the dependence of the yield stress of mild steel upon strain rate. The curve represents an average of experimental data contributed by many authors [11]. It is seen that the yield stress σ_0 rises rapidly with strain rate $\dot{\varepsilon}$ in the range $0 < \dot{\varepsilon} < 10$ but slowly with strain rate above $\dot{\varepsilon} = 10^2$. (At the highest impulse the strain rate is about $200\,\text{sec}^{-1}$.) Hence for small impulses, when the deflections are small enough to consider the membrane effects as small, strain-rate strengthening predominates and for large impulses, when the deflections are large enough to consider the membrane effects large, membrane strengthening predominates. Because of the slow rise in yield stress at higher strain rates the rate of change with impulse of the difference between the δ/R values of aluminum and steel plates settles down to a small quantity as is seen in Fig. 3.

From plate deflection measurements it was found that diametral profiles, normalized at the centers, do not vary greatly with impulse. Some profiles are shown in Fig. 5. This observation indicates that, apart from magnitudes, velocity fields are only moderately sensitive to the level of impulse.

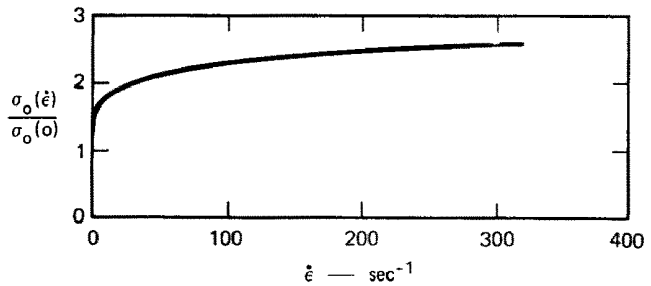

FIG. 4. Variation of mild steel yield stress with strain rate.

Measurements of plate thickness indicate negligible change near the supports and thinning in the central region increasing with impulse from 5 to 9 per cent for aluminum plates and 1 to $4\frac{1}{2}$ per cent for steel plates.

CONSTITUTIVE EQUATIONS

It is assumed that the viscoplastic material can be described as a special case of the constitutive equation [12]

$$\begin{aligned} \dot{\varepsilon}_{ij} &= \gamma^0 \Phi(F) \frac{\partial F}{\partial \sigma_{ij}} \quad \text{for} \quad \sqrt{(J_2)} > k \\ \dot{\varepsilon}_{ij} &= 0 \qquad\qquad\quad \text{for} \quad \sqrt{(J_2)} \leq k \end{aligned} \tag{2}$$

where $\dot{\varepsilon}_{ij}$ and σ_{ij} are components of the plastic strain-rate and stress tensors, γ^0 is a physical constant of the material. In (2), the function F is defined by $F = J_2/k - 1$ where $J_2 = s_{ij}s_{ij}/2$ is the second invariant of the stress deviator with components s_{ij} and k is the yield stress

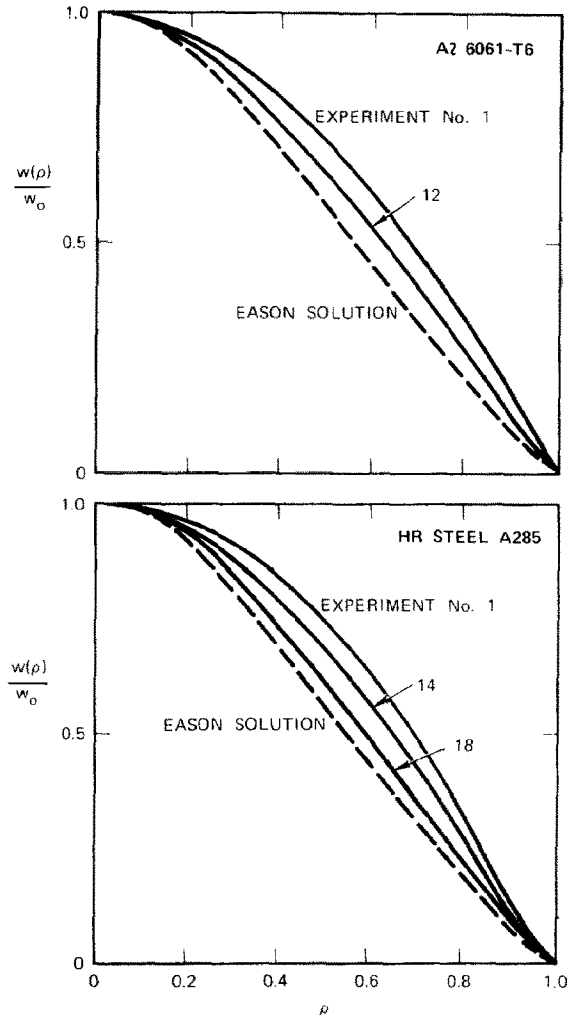

FIG. 5. Final deflection profiles of clamped plates.

in simple shear. The function $\Phi(F)$ should be determined from the results of undimensional tests to describe the material behavior under combined dynamic loading.

The first step in the linearization process is to take $\Phi(F) = F$ in (2), which then becomes

$$\begin{aligned} \dot{\varepsilon}_{ij} &= \gamma(\sqrt{(J_2)}/k - 1)s_{ij}/J_2 \quad \text{for} \quad \sqrt{(J_2)} > k \\ \dot{\varepsilon}_{ij} &= 0 \qquad\qquad\qquad\quad \text{for} \quad \sqrt{(J_2)} \leq k \end{aligned} \tag{3}$$

where $\gamma = \gamma^0/2k$; γ will be called the viscosity constant of the material. These constitutive equations correspond to a straight line of slope $\frac{3}{2}\gamma$ through the point (0, 1) in Fig. 4. As $\gamma \to \infty$, (3) reduce to the Levy–Mises flow rule for rigid–plastic materials, $\dot{\varepsilon}_{ij} = \lambda s_{ij}$.

The second step in the linearization process is to assume that

$$s_{ij}/\sqrt{(J_2)} = \bar{s}_{ij}/\sqrt{(\bar{J}_2)} \qquad \bar{J}_2 = \bar{s}_{ij}\bar{s}_{ij}/2 = k^2$$

where $\bar{s}_{ij}$ denotes components of the plastic stress deviator (on the surface $F = 0$) describing the "state of comparison." Then (2) becomes

$$\begin{aligned} \dot{\varepsilon}_{ij} &= \gamma(s_{ij}-\bar{s}_{ij})/k \quad \text{for} \quad s_{ij} > \bar{s}_{ij} \\ \dot{\varepsilon}_{ij} &= 0 \qquad\qquad\quad \text{for} \quad s_{ij} \leq \bar{s}_{ij}. \end{aligned} \tag{4}$$

Linearization is complete if $\bar{s}_{ij}$ is known. An approximation to $\bar{s}_{ij}$ is given by the plastic stress deviator s^*_{ij} corresponding to the quasi-static flow of a perfectly plastic plate with the same loading and boundary conditions as the viscoplastic plate. It has been shown [8] that s^*_{ij} is a good approximation to $\bar{s}_{ij}$ if the velocity field of the quasi-static problem with perfectly plastic material is similar to the velocity field of the dynamic problem with viscoplastic material. The comparison of normalized deflection profiles from experiment with that from the Eason solution [13] for a perfectly plastic plate with Huber–Mises yield condition demonstrates the similarity of the velocity fields (Fig. 5). It should be noted that the stress tensor s^*_{ij} is not constant at each point in the plate but varies during the deformation process. In general, the directions of the strain-rate vectors appearing in (3) and (4) do not coincide and the linearized constitutive equation (4) belongs to the class of non-associated flow rules.

Since the problem is rotationally symmetric, equations (4) in cylindrical coordinates (r, θ, z) become

$$\begin{aligned} \sigma_r - \sigma^*_r &= (2\dot{\varepsilon}_r + \dot{\varepsilon}_\theta)k/\gamma \\ \sigma_\theta - \sigma^*_\theta &= (2\dot{\varepsilon}_\theta + \dot{\varepsilon}_r)k/\gamma. \end{aligned} \tag{5}$$

Equations (5) include the shell or plate assumption of $\sigma_z = \sigma^*_z = 0$. Use of the Love–Kirchhoff hypothesis in integrating (5) across the plate section yields the flow rule

$$\begin{aligned} M_r - M^*_r &= (2\dot{\varkappa}_r + \dot{\varkappa}_\theta)(k/\gamma)(2h^3/3) \\ M_\theta - M^*_\theta &= (2\dot{\varkappa}_\theta + \dot{\varkappa}_r)(k/\gamma)(2h^3/3) \\ N_r - N^*_r &= (2\dot{\lambda}_r + \dot{\lambda}_\theta)(k/\gamma)2h \\ N_\theta - N^*_\theta &= (2\dot{\lambda}_\theta + \dot{\lambda}_r)(k/\gamma)2h \end{aligned} \tag{6}$$

where $\boldsymbol{M}$, N, $\dot{\varkappa}$, and $\dot{\lambda}$ are bending moments, membrane forces, curvature rates, and extension rates. M^* and N^* satisfy the Huber–Mises yield condition for rotationally symmetric shells [14] and are in static equilibrium for a given boundary value problem.

GEOMETRICAL RELATIONS AND EQUATION OF MOTION

In terms of the horizontal and vertical components of displacement, U and W, the generalized strains are [14]

$$\begin{aligned} \lambda_r &= U' + (W')^2/2 \qquad \lambda_\theta = U/r \\ \varkappa_r &= -W'' \qquad\qquad\quad \varkappa_\theta = -W'/r \end{aligned} \tag{7}$$

where primes denote differentiation with respect to plate radius r. Based upon the experimental results of Griffith and Vanzat [15], the simplifying assumption $U = 0$ is introduced

in (7). Differentiation of (7) with respect to time gives the geometrical relations

$$\begin{aligned} \dot{\lambda}_r &= W'\dot{W}' \qquad \dot{\lambda}_\theta = 0 \\ \dot{\varkappa}_r &= -\dot{W}'' \qquad \dot{\varkappa}_\theta = -\dot{W}'/r \end{aligned} \tag{8}$$

Starting from the Reissner plate equations [16] based on large displacements, small strains, and neglect of rotary inertia, Jones [3] derived equations of motion employing geometrical approximations. Assuming that $U = 0$, the equation of transverse motion combined with the equation for rotational equilibrium of a plate element can be written in the form

$$rM_r'' + 2M_r' - M_\theta' + N_\theta W' + rP - \mu r\ddot{W} = 0 \tag{9}$$

where P is the value of the uniformly distributed pressure.

FORMULATION OF THE MATHEMATICAL PROBLEM

Except at $r = R$ the plate receives an initial transverse velocity $V_0 = I/\mu$, where I is the intensity of the uniformly distributed impulse; thereafter $P = 0$.

In the formulation the following dimensionless variables are employed

$$\begin{aligned} &w = W/R \qquad m_r = M_r/M_0 \qquad m_\theta = M_\theta/M_0 \qquad n_r = N_r/N_0 \qquad n_\theta = N_\theta/N_0 \\ &w_0 = W_0/R \qquad \rho = r/R \qquad p^* = P^*R^2/M_0 \qquad \tilde{I} = IR^2/M_0 t_f \\ &\alpha = \mu R^3/M_0 t_f^2 \qquad \beta = 2R/h = RN_0/M_0 \qquad \tau = t/t_f \qquad t_f = I/P_0^* \end{aligned} \tag{10}$$

where $M_0 = \sigma_0 h^2 = \sqrt{(3)}kh^2$ and $N_0 = 2\sigma_0 h$ are the fully plastic bending moment and membrane force, W_0 is the central deflection, and t_f is the duration of motion according to the bending theory of rigid–plastic plates [9]. The dimensionless form of (9) is

$$\rho m_r'' + 2m_r' - m_\theta' + \beta n_\theta w' - \alpha\rho w = 0 \tag{11}$$

Eliminating $\dot{\lambda}_r$, $\dot{\lambda}_\theta$, $\dot{\varkappa}_r$ and $\dot{\varkappa}_\theta$ between (6) and (8) gives, in dimensionless form the relations

$$\begin{aligned} m_r - m_r^* &= -(2\dot{w}'' + \dot{w}'/\rho)\,4/3\tilde{\gamma}\beta \\ m_\theta - m_\theta^* &= -(\dot{w}'' + 2\dot{w}'/\rho)4/3\tilde{\gamma}\beta \\ n_r - n_r^* &= 2\dot{w}'w'/\tilde{\gamma} \\ n_\theta - n_\theta^* &= \dot{w}'w'/\tilde{\gamma} \end{aligned} \tag{12}$$

where $\tilde{\gamma} = \sqrt{(3)}\gamma t_f$.

Now m_r^*, m_θ^*, n_r^* and n_θ^* satisfy the equilibrium equations of the "state of comparison" which corresponds to the quasi-static flow of a clamped plate under a uniformly distributed pressure p^*. Hence

$$\rho(m_r^*)'' + 2(m_r^*)' - (m_\theta^*)' + \beta n_\theta^* w' - \rho p^* = 0. \tag{13}$$

For small deflections (bending theory), p^* is constant and equals the load carrying capacity of the plate which, with the Huber–Mises yield condition, is $p_0^* = 12{\cdot}5$. For larger deflections, membrane forces come into play and p^* becomes an increasing function of the central deflection w_0.

Figure 5 demonstrates the similarity of the experimental and quasi-static solution profiles. By assuming these deflections to be identical, (13) may be subtracted from (11) to give

$$\rho(m_r - m_r^*)'' + 2(m_r - m_r^*)' - (m_\theta - m_\theta^*)' + \beta(n_\theta - n_\theta)w' + \rho p^* - \alpha\rho\ddot{w} = 0 \tag{14}$$

By using (12) to eliminate the moments and membrane forces, (14) becomes

$$L(w) = \nabla^4\dot{w} + a\alpha\ddot{w} + ap^* + 3\beta^2\dot{w}'w'w''/8 = 0 \tag{15}$$

where $\nabla^2 = \partial^2/\partial^2\rho + \partial/\rho\partial\rho$ is the Laplace operator and $a = 3\tilde{\gamma}\beta/8$.

Because of the unique relationship between generalized stress and strain rate in a viscoplastic material, discontinuities of slope and hinge circles are inadmissible. Hence, at the clamped support $w = w' = 0$ and at the plate center $w' = 0$. Also, from symmetry $m_r = m_\theta$ at the center. The boundary conditions, entirely in terms of w, are thus

$$\begin{aligned} &w'' - w'/\rho = 0, \qquad w' = 0 \quad \text{at} \quad \rho = 0 \\ &w' = w = 0 \qquad\qquad\quad \text{at} \quad \rho = 1. \end{aligned} \tag{16}$$

The initial conditions are

$$w(\rho, o) = 0 \qquad \dot{w}(\rho, o) = \tilde{I}/\alpha \tag{17}$$

BENDING SOLUTION FOR SMALL DEFLECTIONS

When the deflections are small enough to neglect geometry change and membrane forces the governing equation (15) simplifies to the linear parabolic equation

$$\nabla^4\dot{w} + a\alpha\ddot{w} + ap_0^* = 0 \tag{18}$$

In the absence of membrane forces and for a constant pressure term ap_0^* the moments m_r^* and m_θ^* do not change during deformation. In this case the interpretation of the linearized flow rule (6) is that the generalized stress trajectory in bending moment space forms at each point in the plate a closed loop. It has been shown [4, 7] that the assumed non-associated flow rule (6) in the bending theory of dynamically loaded plates leads to results in general agreement with results from experiment and theory based upon (2).

The solution of (18) satisfying the boundary and initial conditions (16) and (17) is

$$w(\rho, \tau) = \frac{I^2R}{p_0^*\mu M_0}\sum_{n=1}^{\infty}\frac{2J_1(\lambda_n)}{\lambda_n^5 I_0(\lambda_n)J_0^2(\lambda_n)}\psi_n(\lambda_n, \rho)[(1 - e^{-\lambda_n^4\tau/\eta})(1 + \eta/\lambda_n^4) - \tau]\eta \tag{19}$$

where

$$\psi_n(\lambda_n, \rho) = I_0(\lambda_n)J_0(\lambda_n, \rho) - J_0(\lambda_n)I_0(\lambda_n, \rho)$$

In (19), $\eta = a\alpha p_0^*/\tilde{I} = 3\sqrt{(3)}p_0^*\gamma\mu R^2/Ih$, J_ν and I_ν are respectively Bessel and modified Bessel functions of the first kind ($\nu = 0, 1$), and the eigenvalues λ_n are roots of the transcendental equation

$$I_0(\lambda_n)J_1(\lambda_n) + J_0(\lambda_n)I_1(\lambda_n) = 0$$

The first nine eigenvalues are

λ_1	λ_2	λ_3	λ_4	λ_5	λ_6	λ_7	λ_8	λ_9
3·19619	6·30635	9·43955	12·5777	15·7165	18·8565	21·9972	25·1380	28·2790

Because of the λ_n^5 term in the denominator of (19) the series is rapidly convergent, provided η is not too large. Since the different eigenfunctions $\psi_n(\lambda_n, \rho)$ reach their maxima at different times $\tau_f^{(n)}$, the plate does not come to rest at all points simultaneously. In the phase plane (ρ, τ) there exists a curve $\xi = \xi(\tau_f)$ which separates regions of viscoplastic flow and rigid behavior.

The equation determining the interface $\xi = \xi(\tau_f)$ is given by $\dot{w}(\xi, \tau_f) = 0$. This curve is shown in Fig. 6 for the chosen value $\eta = 10^2$. It is seen that starting from $\tau = 0{\cdot}5$ a rigid zone propagates from the support at $\rho = 1$ towards the plate center, arriving at $\tau = 0{\cdot}73$. For the intermediate time $0{\cdot}5 < \tau < 0{\cdot}73$, the plate is undergoing deformation within the region $0 < \rho < \xi$ while the outer deformed region $\xi < \rho < 1$ remains rigid. This mode of deformation is analogous to that in a viscoplastic rod during axial impact with a rigid target as described by Ting and Symonds [17].

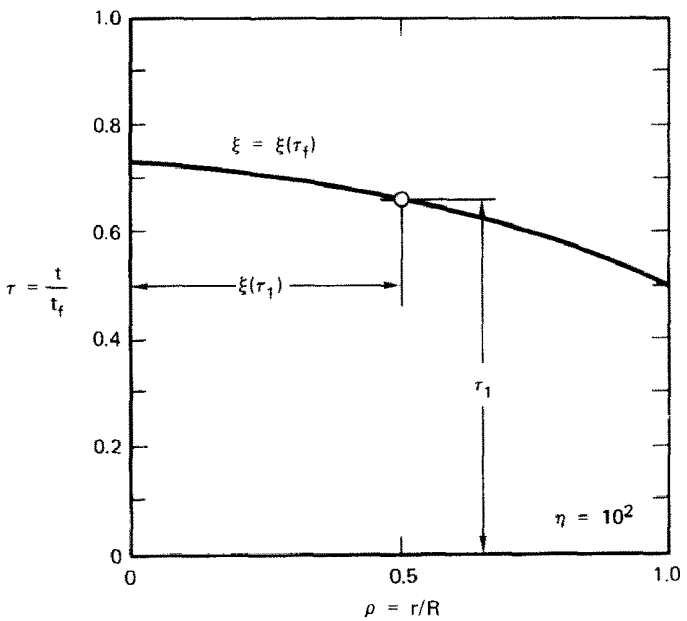

FIG. 6. Rigid and viscoplastic zones.

In Fig. 7 is seen the normalized and dimensionless permanent plate profile obtained from (19) with $\eta = 10^2$. Also shown for comparison is the profile obtained by retaining only the first term of (19). The difference is negligible. The first term approximation is derived by solving $\dot{w}(\xi, \tau_f^{(1)}) = 0$ to give

$$\tau_f^{(1)} = (\eta/\lambda_1^4)\log(1 + \lambda_1^4/\eta) \tag{20}$$

substituting $\tau_f^{(1)}$ into the first term of (19), and using the orthogonal properties of $\psi_n(\lambda_n, \rho)$ to give

$$w(\rho, \tau_f) = (I^2 R/p_0^* \mu M_0)(\lambda_1^4/64)(1-\rho^2)^2\zeta[1 - \zeta\log(1 + 1/\zeta)] \tag{21}$$

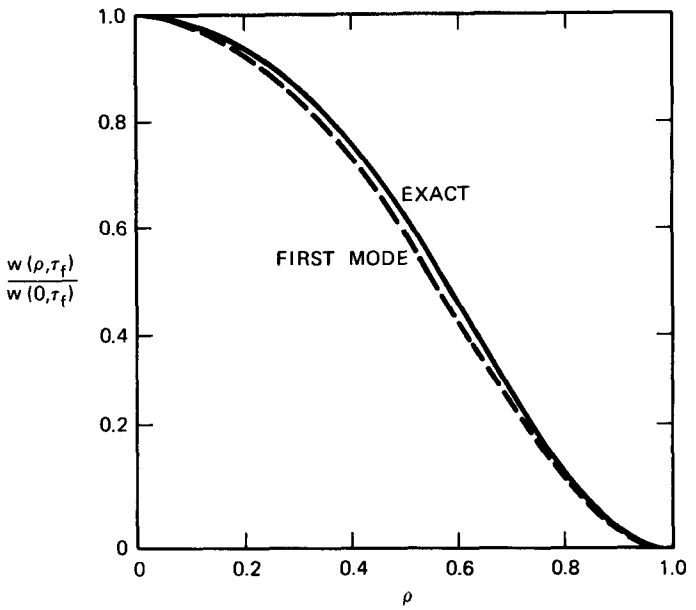

FIG. 7. Plate deflection profiles according to exact solution and first mode approximation.

where $\zeta = \eta/\lambda_1^4 = 3\sqrt{(3)}p_0^*\gamma\mu R^2/Ih\lambda_1^4$. By setting $\rho = 0$, $\lambda_1 = 3{\cdot}196$, and $p_0^* = 12{\cdot}5$ in (21) the central deflection δ is given by

$$\delta/R = 0{\cdot}54(I^2R/8\mu M_0)2\zeta[1-\zeta\log(1+1/\zeta)]. \tag{22}$$

The special case of the rigid–perfectly plastic plate is approached by letting the viscosity constant γ tend to infinity. As $\gamma \to \infty$, (20) shows that $\tau_f^{(1)} \to 1$, that is, the duration becomes $\tau_f = I/p_0^*$ as in the Wang and Hopkins solution. As $\gamma \to \infty$ (hence $\zeta \to \infty$), (22) shows that the central deflection is given by $\delta/R = 0{\cdot}54(I^2R/8\mu M_0)$ which compares favorably with (1).

As $\gamma \to 0$ (hence $\zeta \to 0$), $\delta \to 0$ as it should because a rigid plate is being described. In Fig. 8 is shown the variation with $1/\zeta$ of the coefficient $2\zeta[1-\zeta\log(1+1/\zeta)]$ in (22) and demonstrates the increase in strength of a plate with decrease in the viscosity constant.

STATIC LOAD–DEFLECTION RELATION

Equation (15) governing large deflections of an impulsively loaded plate includes an unknown function $p^*(w_0)$, which is the load–deflection relation of a statically loaded rigid–plastic plate yielding according to the Huber–Mises condition and associated flow rule. Because such a static solution is not available, an approximation to the Calledine [18] solution will be used instead. This solution is shown in Fig. 9. Part of the curve is the parabola

$$p^*/p_0^* = 1+(5/12)(w_0/2h)^2 \quad \text{for} \quad w_0/2h \leq 2/3 \tag{23}$$

while the remainder was obtained by numerical computation. Also shown in Fig. 9 is the approximate membrane solution of Onat and Haythornthwaite [19], which uses the

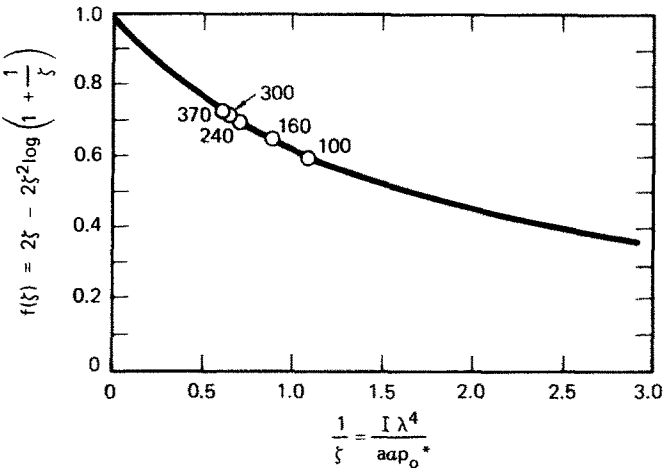

FIG. 8. Influence of viscosity constant on plate deflections.

Tresca yield hexagon circumscribing the Huber–Mises ellipse. The solution is the straight line

$$p^*/p_0^* = 1{\cdot}11(w_0/2h). \tag{24}$$

It is seen in Fig. 7 that with increasing deflection the bending-membrane solution approaches the membrane solution. A very good fit of the Calledine solution over the

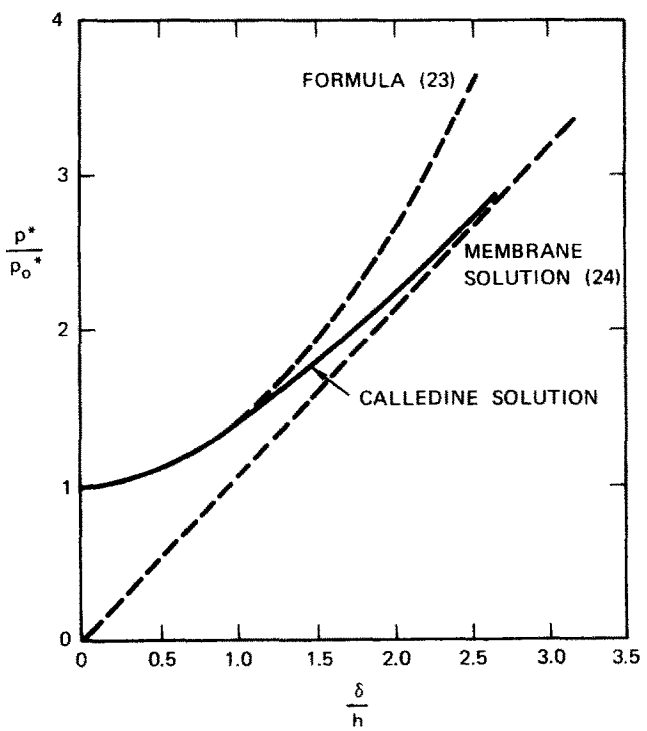

FIG. 9. Static pressure–deflection relations for clamped plate.

entire range of deflections is

$$p^*/p_0^* = [1+(w_0/2h)^2]^{\frac{1}{2}}. \tag{25}$$

BENDING-MEMBRANE SOLUTION FOR LARGE DEFLECTIONS

Because it does not seem possible to obtain the exact solution of (15) an approximate solution is obtained by using the Galerkin procedure. A solution is sought in the form

$$w(\rho,\tau) = \sum_{n=0}^{\infty} w_n(\tau)\psi_n(\rho) \tag{26}$$

where $\psi_n(\rho)$ form a complete system of functions. Functions which satisfy the boundary conditions (16) can be taken as

$$\psi_n(\rho) = (1-\rho^2)^{n+2} \qquad n = 0, 1, 2, \ldots$$

The functions $w_n(\tau)$ are determined from the set of relations

$$\int_0^1 L(w_n)\psi_i(\rho)\rho\,\mathrm{d}\rho = 0 \qquad i = 0, 1, 2, \ldots, n. \tag{27}$$

Because the function $\psi_0(\rho)$ alone gives a good approximation to the normalized and dimensionless deflection profiles of the experiments only the first term in (26) is retained. Note that $\psi_0(\rho) = (1-\rho^2)^2$ is the same as the function occurring in (21), the small deflection solution. Carrying out the integration in (27) leads to the following non-linear ordinary differential equation for the central deflection

$$\ddot{w}_0 + (\lambda/a\alpha)^4)(1+S_1\beta^2 w_0^2)\dot{w}_0 + (10/6\alpha)p^* = 0 \tag{28}$$

where $\lambda = 3{\cdot}2$ and $S_1 = 1/37{\cdot}5$. For small deflections, p^* is constant and the non-linear term $S_1\beta^2 w_0^2$ is small, so the solution of (28) is (21) with λ replacing $\lambda_1 = 3{\cdot}196$. Consequently, the initial velocity $\dot{w}_0(0)$ is taken as the initial velocity from the first mode approximation (21). The initial conditions are therefore

$$\dot{w}_0(0) = (\lambda^4/64)(\tilde{I}/\alpha) \qquad w(0) = 0. \tag{29}$$

Consider first deflections not exceeding the plate thickness for which case the load–deflection relation (23) holds. In the notation of (28), (23) is

$$p^*(w_0) = p_0^*(1+S_2\beta^2 w_0^2)$$

where $S_2 = 1/38{\cdot}4$. By assuming that $S_1 = S_2 = S$, a simple bending-membrane solution is obtained. Employing the change of variables $\ddot{w}_0 = \dot{w}_0\,\mathrm{d}\dot{w}_0/\mathrm{d}w_0$ in (28) and integrating,

$$(a\alpha/\lambda^4)\dot{w}_0 - (a\alpha/\lambda^4)^2(10p_0^*/6\alpha)\log(\dot{w}_0 + 10p_0^* a/6\lambda^4) = -(w_0 + S\beta^2 w_0^2/3) + C \tag{30}$$

where the constant C is determined by the initial conditions (29). When $\dot{w}_0 = 0$, $w_0 = \delta/R$ and thus (30) gives the result

$$\delta/R + (S\beta^2/3)(\delta/R)^3 = 0{\cdot}54(I^2R/8\mu M_0)2\zeta[1-\zeta\log(1+1/\zeta)]. \tag{31}$$

The central deflection of a rigid–plastic plate is obtained by letting $\gamma \to \infty$ (and hence $\zeta \to \infty$) in (31); the term $2\zeta[1-\zeta\log(1+1/\zeta)] \to 1$. To neglect geometry changes, set

$S = 0$ in (31) and obtain (22). By comparing (22) and (31) it is seen that the term describing strain-rate effects is the same for small and large deflections.

For deflections exceeding the plate thickness, the load–deflection relation (23) becomes increasingly inaccurate (Fig. 9) with increasing deflection. The relation (24) can be used if the deflections are large enough to allow the stress distribution to be essentially a purely membrane state. An explicit solution of (28) is now apparently only possible for the limiting case, $\gamma \to \infty$ (and hence $a \to \infty$), describing the rigid plastic plate. This solution is

$$8{\cdot}9(\delta/R)^2 = 0{\cdot}54(I^2R/8\mu M_0). \tag{32}$$

Using the relation (25) covering the entire range of deflections and again restricting the solution of (28) to the limiting case of the rigid–plastic plate, results in

$$(\beta/8)[(\delta/R)\Delta + (4/\beta)^2 \log\{(\beta/4)(\delta/R+\Delta)\}] = 0{\cdot}54(I^2R/8\mu M_0) \tag{33}$$

where

$$\Delta = [(4/\beta)^2 + (\delta/R)^2]^{\frac{1}{2}}.$$

THEORETICAL AND EXPERIMENTAL RESULTS

The effect of geometry change is seen in Fig. 10. Formulas (31), (32) and (33) give the central deflections of rigid–plastic plates ($\gamma = \infty$) and predictions compare favorably with the upper set of experimental points for 6061-T6 aluminum alloy. Formula (33) applies over the whole range of loading and as impulse or deflection is increased the curve bends away from the bending-membrane solution (31) towards the membrane solution (32).

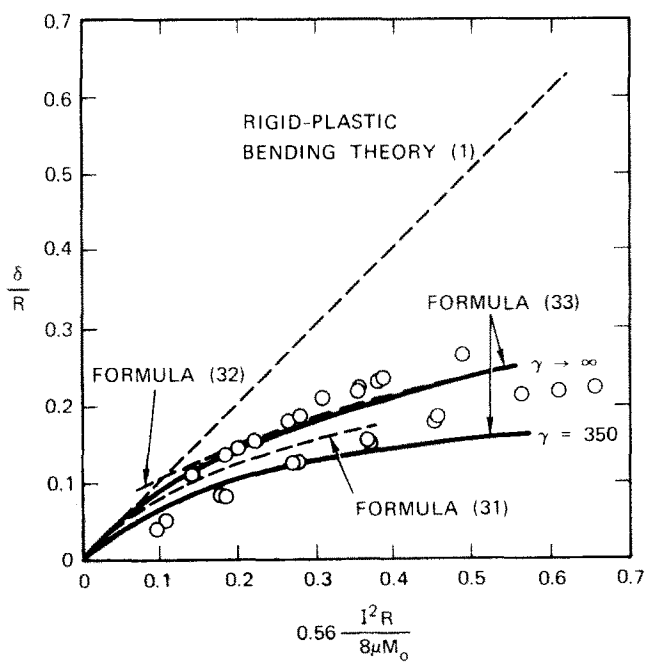

FIG. 10. Experimental and theoretical central deflections for clamped plates.

For the larger impulses the experimental deflections become greater than the theoretical deflections. This trend with increasing impulse is attributable to the clamped support condition of the experiments. It is recalled that the clamping was against rotation only and radially inward displacements were allowed whereas in the theory the simplifying assumption $n = 0$ was used.

The influence of strain rate in the bending and bending-membrane solutions (22) and (31) is described by the function $f(\zeta) = 2\zeta[1 - \zeta \log(1 + 1/\zeta)]$ shown in Fig. 8. A comparison is made with the experimental results shown in Fig. 10 by finding values of the viscosity constant γ necessary for correlation. From two curves fitting the two sets of experimental points, ratios of steel to aluminum plate deflections were calculated at several impulses to cover the range; these ratios range from 0·6 to 0·72. Each deflection ratio was equated to $f(\zeta)$ and the value of ζ was found; this can be done readily by using Fig. 8. From the formula $\zeta = 3\sqrt{(3)}p_0^*\gamma\mu R^2/Ih\lambda_1^4$ the value of γ at each chosen impulse was calculated. Several values of γ are shown in Fig. 8; γ ranges from 100 to 370 sec^{-1}.

A value of $\gamma = 350\,\text{sec}^{-1}$ employed in the bending-membrane solution (31) results in the curve shown in Fig. 10 and gives a fairly good approximation to the experimental results for the steel plates. Agreement over the whole range of deflections cannot be expected with a theory of linear viscosity, as can be deduced from Fig. 4, especially for low impulses and hence low strain-rates. The difference between theory and experiments for high impulses and hence high strain-rates largely attributable to the experimental clamping arrangement which permitted radially inward plastic flow.

CONCLUSIONS

Experiments on impulsively loaded clamped circular plates of 6061-T6 aluminum and H.R. steel A285 show that, relative to strength according to the bending theory of rigid–plastic plates, membrane forces (arising with large deflections) and strain-rate sensitivity have equally important strengthening effects. At low impulses, strain-rate strengthening dominates because of the initial rapid rise of the yield stress of the steel with increasing strain-rate (Fig. 4), and because the deflections are still small enough to keep membrane strengthening small. At higher impulses, membrane strengthening dominates because the yield stress of the steel increases only slightly with increasing strain-rate.

The governing equation (15) has been derived based upon linear viscoplastic behavior and moderately large deflections. Simple formulas for the central deflection have been obtained for the following cases:

(a) Viscoplastic bending action for small deflections (22).
(b) Viscoplastic bending-membrane action for small deflections ($\delta < 2h$) (31).
(c) Rigid–plastic bending-membrane action for large deflections (32).
(d) Rigid–plastic bending-membrane action for all deflections (33).

Correlation of the experimental deflections of the aluminum alloy plates with the predictions of (32) (large deflections) and (33) is reasonably good. Correlation of the deflections of the steel plates with the predictions of (31) (used also for large deflections) is fair (Fig. 10).

To improve this study it is suggested that further similar experiments be carried out but with plate edges clamped against inward radial flow. This additional clamping is

expected to increase the range of dominance of the membrane strengthening and improve correlation of the aluminum plate deflections with the predictions of formulas (32) and (33). Improvements in the theory are necessary for better correlation with steel plate deflections and to explain the small curvatures near the support. However, simple results of practical value would probably be sacrificed in a less approximate theory. One simple modification is to close γ from a straight line in the yield stress–strain-rate plane of Fig. 4 fitting the curve in the higher strain-rate region. A similar technique was employed in [20].

Acknowledgements—The authors are indebted to L. J. Dary for carrying out the experiments and to B. P. Bain for data reduction.

REFERENCES

[1] A. J. WANG, The permanent deflection of a plastic plate under blast loading. *J. appl. Mech.* **22**, 375–376 (1955).
[2] A. L. FLORENCE, Circular plate under a uniformly distributed impulse. *Int. J. Solids Struct.* **2**, 37–47 (1966).
[3] N. JONES, Impulsive loading of a simply supported rigid–plastic circular plate. *J. appl. Mech.* **35**, 59–65 (1968).
[4] T. WIERZBICKI, Impulsive loading of rigid–viscoplastic plates. *Int. J. Solids Struct.* **3**, 635–697 (1967).
[5] N. PERRONE, Impulsively loaded strain-rate sensitive plates. *J. appl. Mech.* **34**, 2 (1967).
[6] N. JONES, Finite deflections of a rigid–viscoplastic strain-hardening annular plate loaded impulsively. *J. appl. Mech.* **35**, 349–356 (1968).
[7] J. M. KELLY and T. R. WILSHAW, A theoretical and experimental study of projectile impact on clamped circular plates. *Proc. R. Soc.* **A306**, 435–447 (1968).
[8] T. WIERZBICKI, Viscoplastic flow of rotationally symmetric shells with particular application to dynamic loading. *J. Mech. Phys. Solids* **3**, 22–37 (1954).
[9] A. J. WANG and H. G. HOPKINS, On the plastic deformation of built-in circular plate under impulsive loading. *J. Mech. Phys. Solids* **3**, 22–37 (1954).
[10] A. L. FLORENCE, Travelling force on a Timoshenko beam. *J. appl. Mech.* **32**, 351–358 (1965).
[11] P. S. SYMONDS, Survey of methods of analysis for plastic deformation of structures under dynamic loading. Division of Engineering, Brown University Report BU/NSRDC, pp. 1–67 (1967).
[12] P. PERZYNA, The constitutive equations for rate sensitive plastic materials. *Q. appl. Mech.* **20**, 321–332 (1963).
[13] G. EASON, Velocity fields for circular plates with the von Mises yield condition. *J. Mech. Phys. Solids*, **6**, 231–235 (1958).
[14] P. G. HODGE, The Mises yield condition for rotationally symmetric shells. *Q. appl. Mech.* **18**, 305–311 (1961).
[15] J. GRIFFITH and H. VANZANT, Large deformation of circular membranes under static and dynamic loading. Paper No. 702 *Ist Int. Congr. Exp. Mech., New York*, Nov. 1–3 (1961).
[16] E. REISSNER, On finite deflections of circular plates. *Proc. Symp. appl. Math.* **1**, 213–219. American Mathematical Society (1949).
[17] T. C. T. TING and P. S. SYMONDS, Longitudinal impact on viscoplastic rods—linear stress–strain-rate law. *J. appl. Mech.* **31**, 199–207 (1964).
[18] C. R. CALLEDINE, Simple ideas in the large-deflection plastic theory of plates and slabs. *Engineering Plasticity*, edited by J. HEYMAN and F. A. LECKIE. Cambridge University Press (1968).
[19] E. T. ONAT and R. M. HAYTHORNTHWAITE, The load carrying capacity of circular plates at large deflection. *J. appl. Mech.* **23**, 49–55 (1956).
[20] A. L. FLORENCE, Buckling of viscoplastic cylindrical shells due to impulsive loading, *AIAA Jnl* **6**, 532–537 (1968).

(*Received* 30 *June* 1969)

Абстракт—Излагаются эксперименты, касающиеся поведения защемленных круглых пластинок, изготовленных из алюминиего сплава 6061–*T6* и стали *A 285* высокого сопротивления, подверженных пействию одномерно расположенных импульсов. Зти импульсы вызывают постоянные центральные прогибы, имеющие велиуину одной до некоторых толщин пластнпки. Предлагается вязкоупругая теория пластинок, учитывающоя большие ирогибы. В кауестве специального случая, теория заключает жестко-идеально пластическую пластинку. Путем корреляции предусмотренных и экспериментальных прогибов пластинок, изготовленных из алюминия нечувствительного к скорости деформации и стальных пластинок, чувствительных к скорости деформации, определется, что эффекты больших прогибов /которые дают рост, имеющим большие знапение, мембранным усилиям/ и чувствительность к скорости деформации являются сравнительно ответственные прогибам расположенным ниже этих, которые прелсказывает моментная теория жестко-идеально пластических пластинок.